SHORT-RANGE WAKEFIELD CALCULATIONS FOR THE ION CLEARING ELECTRODES IN THE CORNELL ENERGY RECOVERY LINAC

A Thesis

Presented to the Faculty of the Graduate School

of Cornell University

in Partial Fulfillment of the Requirements for the Degree of

Master of Science

by

Yi Xie

August 2007

ABSTRACT

The presence of trapped ions in the Cornell Energy Recovery Linac (ERL) can lead to beam halo, particle loss, optical errors, or transverse and longitudinal instabilities. DC clearing electrodes that create a sufficient voltage to draw ions out of the beam potential are considered to be the most easily applicable measure to cure these effects. However, due to the short length of electron bunches in the ERL running modes, the power dissipated by the clearing electrodes can significantly damage these. I have calculated the short-range wakefields of different types of clearing electrodes and concluded that a tapered electrode design can be used.

BIOGRAPHICAL SKETCH

Yi Xie was born February 12, 1982 in Danjiangkou, Hubei province of China to Risheng Xie and Huilan Zhou. He attended First Dangjiangkou High School and graduated in 1998. After four years study at Chongqing University of Posts and Telecom, he obtained a Bachelor Degree in Telecommunication Engineering.

At the age of 20, he changed his career from engineering to physics and was enrolled in School of Physics, Peking University. He joined the accelerator physics group in the Institute of Heavy Ion Physics and worked on a project which used Radio Frequency Quadrupole (RFQ) to perform Accelerator Mass Spectrometry (AMS). He coauthored a Chinese patent and several papers on that RFQ-AMS project and obtained a Master of Engineering degree in Accelerator Technology.

In 2005, he entered the Physics Department of Cornell University as a Ph.D student. From 2005-2007, he worked with Prof. Georg Hoffstaetter on the ion clearing methods and ion clearing electrodes wakefields calculations for the Energy Recovery Linac (ERL) project. In the forthcoming summer, he will work in the Radio Frequency Super-conducting group led by Prof. Hasan Padamsee as a graduate research assistant.

For his future plans, Yi is not ruling out writing film critics for the Chinese movie industry.

ACKNOWLEDGEMENTS

First I would like to thank my advisor Prof. Georg Hoffstaetter. He taught me about accelerator physics and about the ERL project through our friendly discussions. Then I should thank every one in the Wilson accelerator physics community. Ivan Bazarov, Mike Billing, Yulin Li, David Sagan and Rongli Geng are very helpful whenever I have questions. As my wakefields computation research progressed, I benefited a lot from Haipeng Wang (JLAB), Martin Dohlus (DESY), Igor Zagorodnov (DESY), Graeme Burt and Carl Beard (Lancaster University). Also I thank my fellow students Chris Mayes, Changsheng Song and Brandon Buckley for their stimula tions. Finally, I thank my family in China for their love and support.

TABLE OF CONTENTS

1 Introduction **1**
1.1 Outline . . . 2

2 Ion effects in the ERL **3**
2.1 The Cornell ERL development . . . 3
2.2 Ion production and neutralization . . . 6
2.3 Critical Mass . . . 7
2.4 Electrostatic potential of the beam . . . 8
2.4.1 Circular vacuum chamber . . . 9

3 Wakefield calculations of the ion clearing electrodes **14**
3.1 Theory of wakefields . . . 14
3.1.1 Wake fields . . . 14
3.1.2 Longitudinal wake functions . . . 15
3.1.3 Longitudinal wake potentials . . . 15
3.1.4 Longitudinal loss factor . . . 16
3.1.5 Transient heating due to short-range wakefields . . . 17
3.1.6 Resonant excitation due to long-range wakefields . . . 17
3.2 MAFIA simulation . . . 19
3.2.1 The geometry and meshing . . . 19
3.2.2 Boundary conditions and particle beams . . . 21
3.2.3 Wake Monitors and post-processing . . . 21
3.3 Ion clearing electrodes from JLAB . . . 22
3.4 Initial design of ion clearing electrodes for the ERL . . . 24
3.5 Tapered and diamond-shape ion clearing electrodes design . . . 29
3.5.1 Numerical dispersion errors . . . 31
3.5.2 Tapering effects . . . 32
3.5.3 Gap width dependence . . . 34
3.6 A diamond-shape ion clearing electrode design with a smaller beam pipe radius . . . 35

4 Conclusion **37**

Bibliography **38**

LIST OF TABLES

2.1 ERL parameter sets for short-term goals (A-C) and for longer-term goals (D-E). 5
2.2 The parameters of collision ionization for the main molecular species at the ERL 7

LIST OF FIGURES

2.1 An schematic layout of Cornell ERL 4
2.2 An elliptic cross-section beam in a circular vacuum chamber 9
2.3 Electrostatic potential at the center of the beam in a circular chamber 10
2.4 Locations of ion clearing electrodes (0-1150m) 12
2.5 Locations of ion clearing electrodes (1150-1725m) 13

3.1 Wake fields in an accelerator 14
3.2 Meshing in MAFIA 20
3.3 An ion clearing electrode from JLAB 22
3.4 MAFIA model of an ion clearing electrode from JLAB 23
3.5 Mesh variation for a 5mm Gaussian bunch in Jlab ion clearing electrodes. Note that 5 mesh points per bunch length is sufficient in this structure. 23
3.6 Mesh variation for a 1mm Gaussian bunch in Jlab ion clearing electrodes 24
3.7 Wake potentials for different bunch lengths in Jlab ion clearing electrodes 25
3.8 Longitudinal loss factors for different bunch lengths in Jlab ion clearing electrodes 25
3.9 Ion clearing electrode for the ERL; design (1). 26
3.10 MAFIA model of the ion clearing electrode design (1) 27
3.11 Wake potentials for different bunch lengths in ion clearing electrodes design (1) 27
3.12 Longitudinal loss factors for different bunch lengths in ion clearing electrodes design (1) 28
3.13 MAFIA model of a tapered clearing electrode design (2) 29
3.14 A diamond-shape clearing electrode design (2) 30
3.15 MAFIA model of the diamond-shape clearing electrode design (2) . 30
3.16 Longitudinal wake potentials for different bunch lengths in the diamond-shape clearing electrode, design (2) 31
3.17 Longitudinal loss factors for different bunch lengths in the diamond-shape clearing electrode, design (2) 32
3.18 Longitudinal wakefields for different mesh sizes in MAFIA 33
3.19 Longitudinal loss factors changed with the mesh size in MAFIA . . 33
3.20 Longitudinal loss factor change with tapering angle in the diamond-shape clearing electrode 34
3.21 Longitudinal loss factor change with the gap width in the diamond-shape clearing electrode 35
3.22 Longitudinal wake potentials for different bunch lengths in the diamond-shape clearing electrode with a smaller beam pipe radius, design (3) 36

3.23 Longitudinal loss factors for different bunch lengths in the diamond-shape clearing electrode with a smaller beam pipe radius, design (3) 36

Chapter 1

Introduction

X-ray beams generated by particle accelerators are widely used in resolving the structure of matter down to the level of atoms and molecules. An electron beam with high current and small emittance is necessary to obtain high brilliance x-ray beams. By preserving the extremely small emittance produced by a linear accelerator, the energy recovery linac (ERL) will produce brighter and much shorter x-ray pulses compared to traditional storage ring light sources.

However, for a high beam current such as 100 mA and high energy such as 5 GeV, the resultant power will be 500 MW which can't be afforded. So in the ERL case, the electron beam is sent on a second pass through the linac. By having this bunch arrive at the correct RF phase for deceleration, the energy is extracted by the linac structure and is given to the next bunch.

Ions produced by the collision between circulating electron beams and residual gas can be very harmful. It can lead to electron beam-emittance blow-up, coupling of horizontal and vertical motions and beam instabilities. Therefore, DC electrodes have to be used to draw the ions out of the electron beam potentials.

However, the DC electrodes will produce so-called short-range wakefields which disturb the electron beams by causing energy spread within the electron bunches. Also the short-range wakefields may deposit power to the accelerator structure and over-heat the electrodes.

1.1 Outline

The thesis begins with a brief introduction of the Cornell ERL project. In the second chapter the electrostatic beam potentials for the circular vacuum chamber along the ERL will be calculated to determine the locations of the ion clearing electrodes. In the third chapter, the short-range wakefield properties of different designs of ion clearing electrodes will be computed by an EM field solving code. In the last chapter, ion-clearing electrode design considerations will be given based on our short-range wakefield simulations.

Chapter 2

Ion effects in the ERL

2.1 The Cornell ERL development

Cornell is going to build a new synchrotron radiation source called Energy Recovery Linac (ERL). Fig. 2.1 is the schematic layout of the ERL planned. A 10 MeV injector (1) injects an electron beam into a 2.5 GeV linac (2). Then the beam goes through a return loop (3) and enters a second 2.5 GeV linac. The two linacs are located in the same tunnel to save civil engineering costs. By going through an injection arc (5) in the south, the electron beam goes into the CESR ring (6) and comes back to the first linac (1) through another arc (7)in the north. Since the electrons arrive at the decelerating phase of the electromagnetic field in the first linac (1), the electron beam gets decelerated to 2.5 GeV. It goes through the return loop (3) into the second 2.5 GeV linac and gets decelerated again to 10 MeV and goes into the beam dump (8).

Table. 2.1 [1] is the parameter set for the Cornell ERL x-ray source. Each column represents one mode of operation. There are three short-term running goals which we propose for the Cornell ERL after a reasonable commissioning time and two longer-term running goals that might be achievable with ERL technology.

From the parameter table, we notice that ERL requires very small transverse emittances. However, the ions generated by the beam interaction with the residual gas in the accelerator vacuum chamber can significantly dilute the emittances. Traditionally, there are two major methods to dealing with the ion accumulation [2].

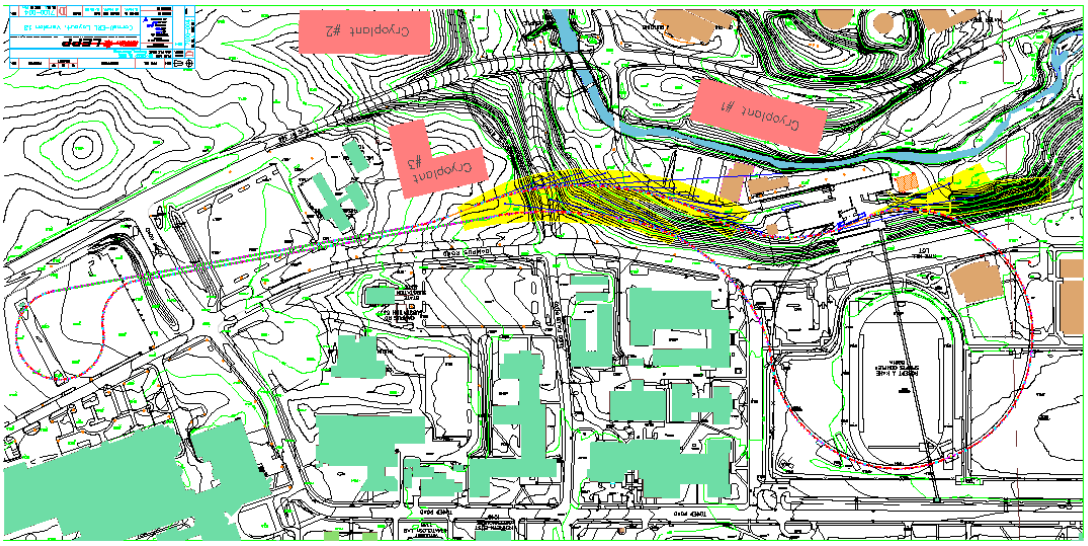

Figure 2.1: An schematic layout of Cornell ERL

Table 2.1: ERL parameter sets for short-term goals (A-C) and for longer-term goals (D-E).

Modes	(A)Flux	(B)High-Coherence	(C)Short-Pulse	(D)Ultra High-Coherence	(E)Ultra Short-Pulse	Unit
Energy	5	5	5	5	5	GeV
Macropulse current	100	25	1	100	1	mA
Bunch charge	77	19	1000	77	10000	pC
Repetition rate	1300	1300	1	1300	0.1	MHz
Transverse emittance (norm.rms)	0.3	0.08	5.0	0.06	5.0	mm.mrad
Transverse emittance (geometric at 5GeV)	31	8.2	511	6.1	511	pm
Bunch length (rms)	2000	2000	50	2000	20	fsec
Intrabunch energy spread (fractional;rms)	2E-4	2E-4	3E-3	2E-4	3E-3	

1. Gaps between electron bunch trains either let the ions drift out of the beam or let the ions experience unstable oscillations.

2. Using DC or RF electrodes to provide a transverse electric field which draws ions out of the beam region.

It was decided the most easily applicable way to eliminate ions in Cornell ERL is to use DC electrodes [3].

2.2 Ion production and neutralization

Ions can be generated in the inelastic collisions of the circulating electron beam with the molecules of residual gas, by tunnelling ionization due to the collective electric field of the bunch, in the Compton scattering of the synchrotron radiation on the electrons of residual gas molecules, and the ion desorption from the wall of the vacuum chamber. The first mechanism of ion production is the main one.

The cross section of the inelastic collision can be written as

$$\sigma_{col} = 4\pi\lambda_c^2\beta^2 C + 2M^2[\ln(\beta\gamma) - \frac{1}{2}], \tag{2.1}$$

where C and M^2 depend on the gas [4], $\lambda_c = \hbar/(m_e c)$ is the Compton wavelength of the electron, γ is the relativistic factor, and c is the speed of light.

The residual gas in the ERL is mainly composed of molecular hydrogen, carbon monoxide, carbon dioxide and a small amount of other molecular species. Tab. 2.2 shows the cross section σ_{col} and the neutralization time τ_{col} at the ERL energies [3].

The neutralization time τ_{col}, defined as the average time it takes for one circu-

Table 2.2: The parameters of collision ionization for the main molecular species at the ERL

Ion	Atomic number	σ_{col} (m^2),10MeV	σ_{col} (m^2),5GeV	τ_{col} (s),5GeV
H_2	2	2.0E-23	3.1E-23	5.6
CO	28	1.0E-22	1.9E-22	92.7
CH_4	44	1.2E-22	2.0E-22	85.2

lating particle to create one ion, is [3]

$$\tau_{col} = \frac{1}{\rho_{gas}\sigma_{col}c}, \tag{2.2}$$

where the gas density ρ_{gas} is computed from the gas pressure p_{gas}, the Boltzmann constant k_B and the temperature T by $\rho_{gas} = \frac{p_{gas}}{k_B T}$. From the neutralization times of the Table. 2.2, the neutralizing ion beam will mostly consist of H_2^+ ions.

2.3 Critical Mass

Positive ions are trapped by the electron beam if they are heavy enough i.e. if their mass A (in atomic mass units) is larger than the critical mass [5]

$$A_{ion} \geq \frac{n_e r_p}{4\sigma_y(\sigma_x + \sigma_y)}\Delta L_g \tag{2.3}$$

with the classical proton radius $r_p = \frac{e^2}{4\pi\epsilon_0 m_p c_{light}^2} = 1.5 \times 10^{-18}$m. ΔL_g is the gap distance between bunches. ϵ_0 is the vacuum permittivity. In the operation modes 1 and 2, ΔL_g=0.23m. For mode 3, the bunches are separated by 1μs so ΔL_g= 300m.

With the beams transverse size $\sigma = \sqrt{\epsilon\beta_{aver}} = \sqrt{\epsilon_N\beta_{aver}c/v\gamma}$, The critical mass for mode 1 and 2 is 0.004. Here ϵ and ϵ_N are the unnormalized and normalized emittance. The average beta function β_{aver} is assumed to be 50m. The velocity of

the beam is v. That means no ion can escape from the beam potential. For mode 3 the result is 13.99 which means that only particles lighter than 14 atomic mass units will escape.

2.4 Electrostatic potential of the beam

Because ions are generated with very small kinetic energy, according to the Lorentz force formula the magnetic field generated by the electron beam does not strongly influence the ions. So the electric field of the beam contributes mostly to the ion trapping. The beam pipe is grounded at zero potential. Variations in vacuum chamber shape and size, as well as the change in beam size, will cause the electrostatic potential at the beam center to vary along the accelerator. Ions are trapped transversely by the beam field, but because of the longitudinal potential variation, ions may drift longitudinally depending on where they are born. This requires the clearing electrodes to be properly placed at the right positions to avoid local ion accumulations. In addition, the electric field generated by the electrodes must at least overcome the local maximum electric field due to the particle beams. Therefore, a detailed knowledge of the beam potential along the ERL is needed to determine the optimum positions and voltages for the clearing electrodes.

Because the beam size usually changes longitudinally on a scale much larger than that of the transverse beam size and vacuum pipe diameter, we reduce finding the potential to a 2 dimensional problem. At any location longitudinally, we compute the potential of an infinitely long beam inside an infinitely long conducting boundary with the local transverse geometry.

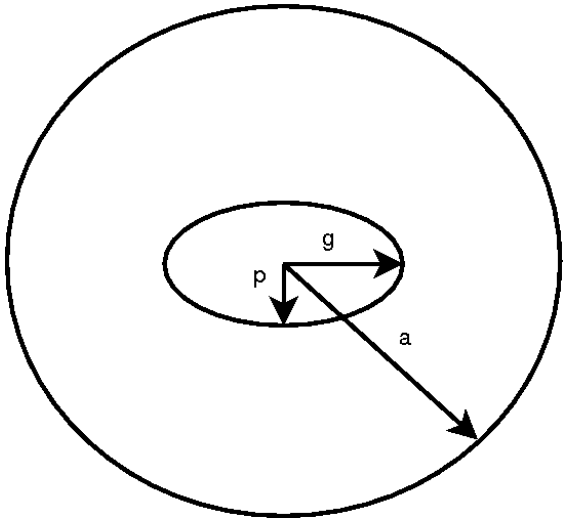

Figure 2.2: An elliptic cross-section beam in a circular vacuum chamber

2.4.1 Circular vacuum chamber

Fig. 2.2 shows an elliptic cross-section electron beam in a circular cross-section vacuum chamber. The charge density is ρ_0, $2g$ and $2p$ are the two axes of the beam ellipse, a is the radius of the vacuum chamber.

The potential has a minimum at the center of the beam [6]

$$\Phi_{max} = -\frac{\rho_0 g p}{2\epsilon_0}(\frac{1}{2} + \ln\frac{2a}{g+p}). \tag{2.4}$$

Considering that the r.m.s widths of ellipse of uniform density is $\sigma_x = g/2$, $\sigma_y = p/2$, eqn. 2.4 with the transverse r.m.s beam sizes σ_x and σ_y becomes:

$$\Phi = -\frac{2\rho_0\sigma_x\sigma_y}{\epsilon_0}(\ln\frac{a}{\sigma_x+\sigma_y} + \frac{1}{2}). \tag{2.5}$$

The electron charge density ρ_0 is related to the beam current I by

$$\rho_0 = \frac{I}{v\pi\sigma_x\sigma_y}. \tag{2.6}$$

Here v is the velocity of the beam.

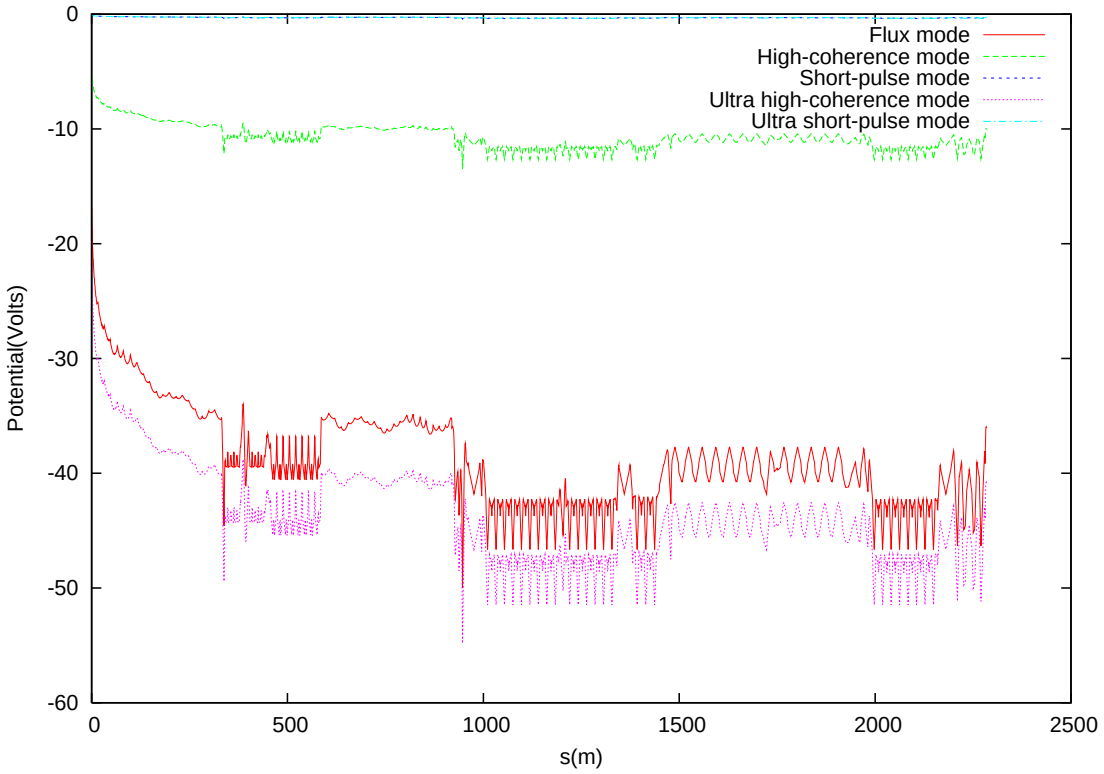

Figure 2.3: Electrostatic potential at the center of the beam in a circular chamber

The transverse rms beam sizes $\sigma_{x,y}$ are related to the nominal emittances $\epsilon_{Nx,Ny}$ of the beam by

$$\sigma_{x,y} = \sqrt{\frac{c\epsilon_{Nx,Ny}}{v\gamma}\beta_{x,y}}. \tag{2.7}$$

Here $\beta_{x,y}$ are the betatron amplitude functions, γ is the relativistic factor. Thus the equation used in the actual numerical calculation for the beam potential becomes $(v \sim c)$

$$\Phi = -\frac{2I}{\pi\epsilon_0 c}(\ln\frac{a\sqrt{\gamma}}{\sqrt{\epsilon_{Nx}\beta_x}+\sqrt{\epsilon_{Ny}\beta_y}}+\frac{1}{2}). \tag{2.8}$$

For the five working modes discussed above, for example, the high brilliance mode with current $I = 25$mA and nominal emittances of $\epsilon_{Nx} = \epsilon_{Ny} = 0.08$mm.mrad, leads to the beam potentials shown in Fig. 2.3.

Electrostatic ion clearing electrodes produce a DC electric field that draws ions out of the electron beam's potential.The four graphs in Fig. 2.4 and Fig. 2.5 show

the beam potential for the flux mode. The ion clearing electrodes need to be put at the beam potential minimums. By counting all the minimums, the number of ion clearing electrodes is expected to be about 153.

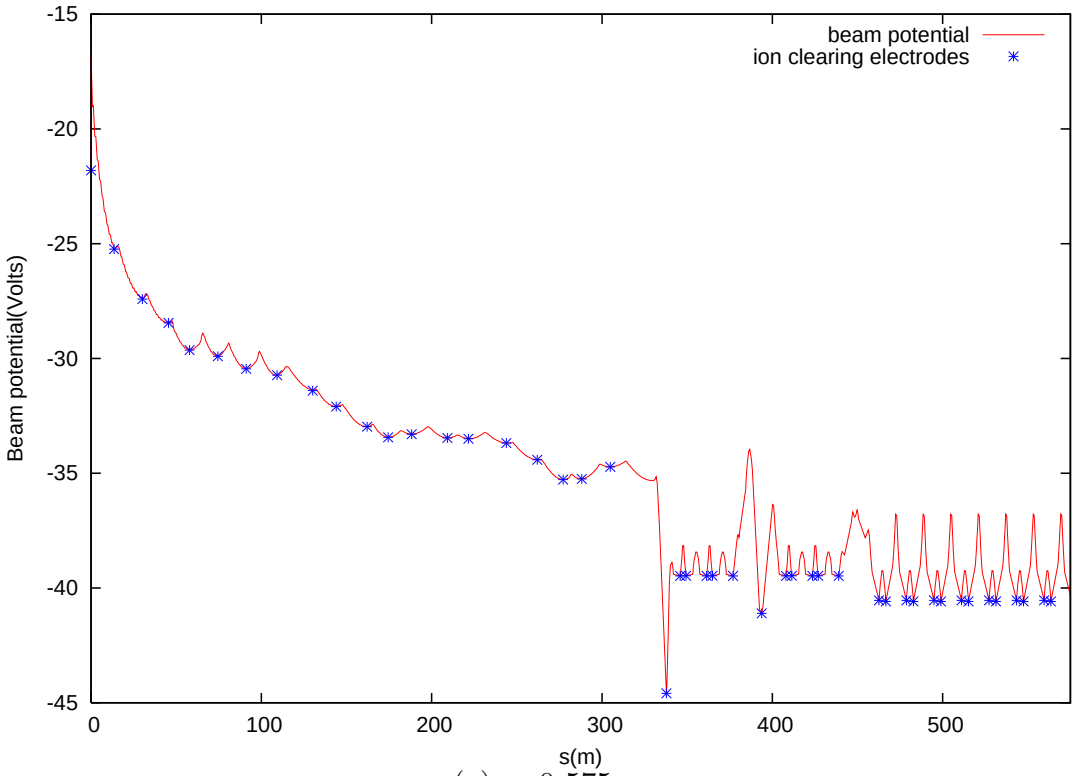

(a) s=0-575m

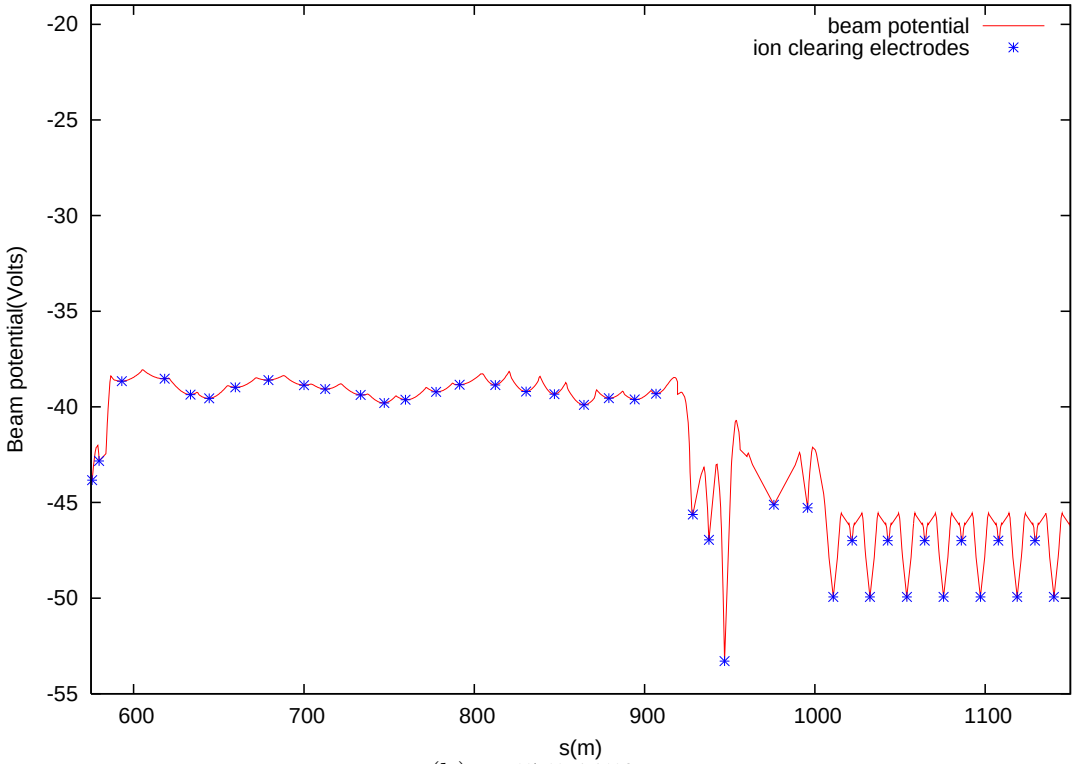

(b) s=575-1150m

Figure 2.4: Locations of ion clearing electrodes (0-1150m)

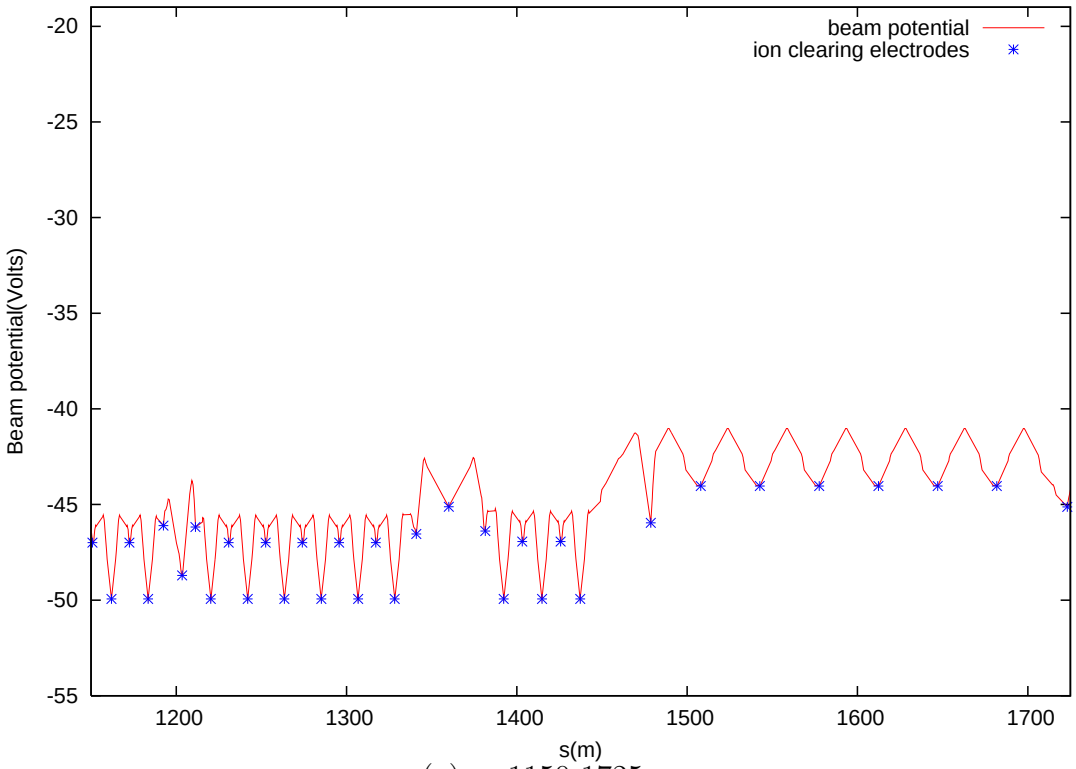

(a) s=1150-1725m

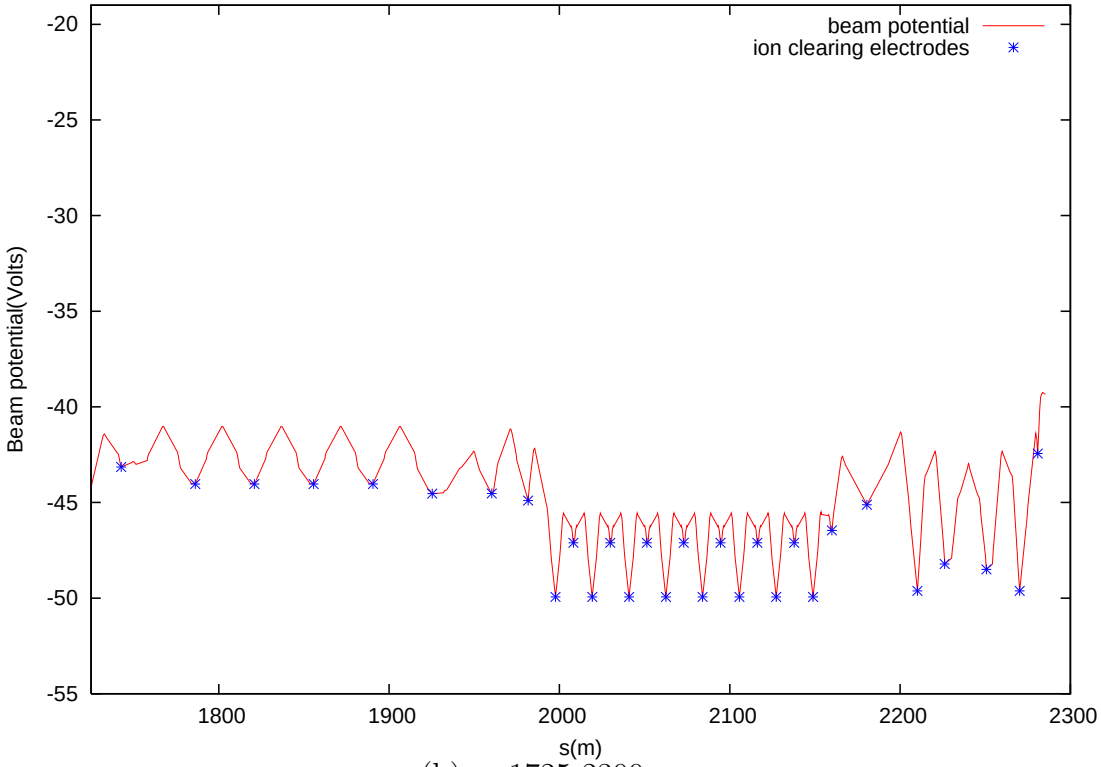

(b) s=1725-2300m

Figure 2.5: Locations of ion clearing electrodes (1150-1725m)

Chapter 3

Wakefield calculations of the ion clearing electrodes

3.1 Theory of wakefields

3.1.1 Wake fields

A charged particle beam generates EM fields that are called wake fields since they are usually behind the leading bunch at any cross-section variation of the vacuum chamber. Fig. 3.1 shows how the leading bunch exerts a wakefield on the trailing bunch where Δt_b is the bunch separation time.

Although wake fields may get trapped or may propagate in the vacuum chamber, inevitably they will react back on the beam and interact with the vacuum chamber structure. They may lead to energy loss, to beam instabilities, or produce undesirable secondary effects such as excessive heating of sensitive components at or near the vacuum chamber wall. For example, ion clearing electrodes may get very hot when a very short electron bunch passes by. Therefore we must have a

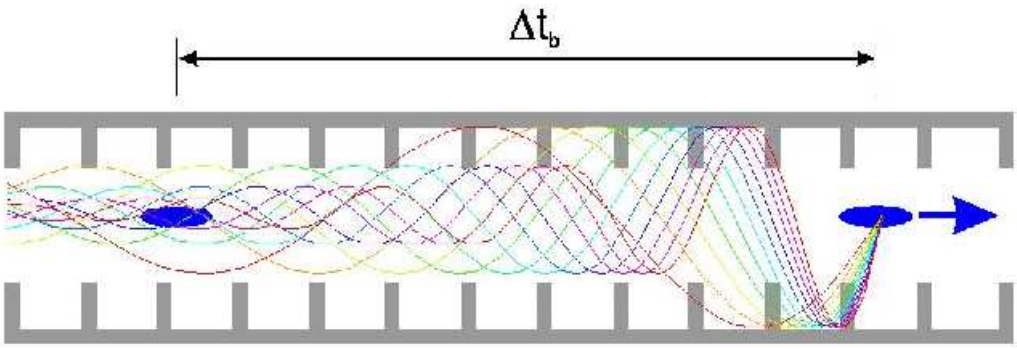

Figure 3.1: Wake fields in an accelerator

good knowledge of these wake fields and of their interactions.

3.1.2 Longitudinal wake functions

The longitudinal wake function of a structure is obtained by integration of the EM forces acting on a trailing charge at a distance s behind a leading charge at a transverse offset $\vec{r}_e$ from the leading charge's trajectory assumed to be parallel to the axis of the structure. Since the magnetic force is perpendicular to the direction of the particle motion it does not contribute to energy changes, so the longitudinal wake function is calculated by integrating only over the electric field component E_z normalized by the charge q [7].

$$G_{\parallel}(\vec{r}_b, \vec{r}_e, s) = -\frac{1}{q}\int_{-\infty}^{\infty} dz E_z(\vec{r}_b, \vec{r}_e, z, t = \frac{z+s}{c}), \tag{3.1}$$

Here $\vec{r}_b$ is the transverse offset of the leading charge relative to the design trajectory. The minus sign is introduced so that the positive longitudinal wake functions correspond to an energy loss of the trailing charge if both the leading and trailing charge have the same sign of charge. The dimensions of the wake function is V/C= Ω/s, for real accelerator structures the units V/pC= 10^{12}V/C are commonly used.

3.1.3 Longitudinal wake potentials

The longitudinal wake potential is defined as integrals over the EM forces exerted by wake fields at the position of a test charge following on the same trajectory. Unlike the longitudinal wake function, the leading charge is replaced by a bunch of particles, of finite length, and the distance to the test charge s is measured from

the bunch center. Therefore the wake function is the wake potential of a delta-function distribution, and can be seen as Green function for the wake potential of a finite particle distribution in the same structure.

For a bunch of arbitrary shape, the longitudinal wake potential can be obtained from the convolution of the wake function $G_{\parallel}(s)$ with the normalized line density $\lambda(s)$,

$$W_{\parallel}(s) = \int_{-\infty}^{s} ds' \lambda(s') G_{\parallel}(s - s') = \int_{0}^{\infty} ds' \lambda(s - s') G_{\parallel}(s'). \tag{3.2}$$

Here $G_{\parallel}(s)$ has only been evaluated for positive s, because there is no significant field ahead of a bunch for relativistic particles.

For a Gaussian bunch with $\lambda(s)$ given by

$$\lambda(s) = \frac{1}{\sqrt{2\pi}\sigma} \exp(-\frac{(s - s_0)^2}{2\sigma^2}). \tag{3.3}$$

The longitudinal wake potential is then given by

$$W_{\parallel}(s) = \frac{1}{\sigma\sqrt{2\pi}} \int_{0}^{\infty} dt G_{\parallel}(s) \exp(-\frac{(s - s_0)^2}{2\sigma^2}). \tag{3.4}$$

In practice it is difficult to calculate wake functions of point charges except for a few simple geometries which can be solved analytically. Therefore the wake potentials of finite bunches are calculated by numerical EM simulation codes such as MAFIA [9].

3.1.4 Longitudinal loss factor

The longitudinal loss factor is introduced to simplify the calculation of the energy loss of bunched beams passing through vacuum chambers. The energy change of a bunch passing through a structure can be written as:

$$\Delta E = -\kappa_{\parallel} q^2, \tag{3.5}$$

where the proportionality factor $\kappa_{\parallel}$ is called the longitudinal loss factor.

The longitudinal loss factor depends not only on the structure, but also on the bunch shape, especially on the bunch length. It can also be obtained by integrating the product of the wake potential $W_{\parallel}(s)$ and the line charge density of the particle distribution $\lambda(s)$ [7]:

$$\kappa_{\parallel} = \int_{-\infty}^{\infty} ds W_{\parallel}(s)\lambda(s). \tag{3.6}$$

3.1.5 Transient heating due to short-range wakefields

The power lost by the bunch goes to the traversed structure. Power loss due to short-range wakefields is a "single-pass" effect, which means the effects of successive bunches do not add up coherently. So it is sufficient to calculate the energy loss for one passing bunch. The heating power P for a current I of many bunches is then given by

$$P = \frac{N_b}{T_{rev}}\Delta E = \frac{N_b}{T_{rev}}\kappa_{\parallel} q^2 = \kappa_{\parallel} q I, \tag{3.7}$$

with the charge per bunch q, the number of bunches in the accelerator N_b and the revolution frequency $1/T_{rev}$.

3.1.6 Resonant excitation due to long-range wakefields

Long-range wakefields are dominated by the interaction of the beam with resonant EM field modes in an accelerator structure. Successive beam bunches may cause resonant excitation of EM fields when one of the beam's spectral lines is in resonance with one of the structure's EM field modes.

When one of the structure's EM field modes is driven by the successive bunches

coherently, the beam can induce a voltage

$$V_n = \int dz E_{z,n}(z) e^{i\frac{\omega_n}{v}z}, \tag{3.8}$$

where $E_{z,n}(z)$ is the longitudinal component of the electric field $\vec{E_n}$ of that mode.

The induced voltage $V_n(t)$ into a mode with frequency ω_n after one bunch with charge q passing by can be found as:

$$V_n(t) = 2q\kappa_{\|n} \cos(\omega_n t_b) \exp(-\frac{\omega_n}{2Q_n} t_b), \tag{3.9}$$

where bunch separation is t_b, quality factor of that mode is Q_n.

The induced voltage $V_n(mt_b)$ after m bunches passing by is:

$$V_n(mt_b) = 2q\kappa_{\|n} \sum_{k=1}^{m} \cos(\omega_n k t_b) \exp(-\frac{\omega_n}{2Q_n} k t_b). \tag{3.10}$$

For the worst case all bunches are in phase with period of that mode $\omega_n t_b = 2\pi l$ where l is integer. Let $m \to \infty$,

$$V_n(\infty) = 2q\kappa_{\|n} \sum_{k=1}^{\infty} \exp(-\frac{\omega_n}{2Q_n} k t_b) = \frac{2q\kappa_{\|n} \exp(-\frac{\omega_n}{2Q_n} t_b)}{1 - \exp(-\frac{\omega_n}{2Q_n} t_b)} \approx 2q\kappa_{\|n} \frac{2Q_n}{\omega_n t_b}. \tag{3.11}$$

Therefore the power losses due to the resonant excitation into wall current or heating is

$$P_n = V_n I = 4\kappa_{\|n} \frac{Q_n}{\omega_n} I^2, \tag{3.12}$$

where $I = q/t_b$ is the beam current.

The modal loss factor and frequency are determined by the geometrical shape of the structure. The quality factor Q_n depends on material properties. They are usually calculated by some computer programs for EM fields in the frequency domain.

3.2 MAFIA simulation

MAFIA [9] has a T3 module that enable the user to record the wakefields as a function of s (the distance behind the leading particle). The orientation of the s-axis is opposite to the moving direction of the particles.

There are at least two techniques of calculating the wake field, the direct and the indirect method; The direct integration technique computes the time integral over the EM forces in the specified range from the computed fields. This method is limited by numerical noise. The indirect method calculates the EM field at the location of the walls of a surrounding cylinder to calculate the wake integral. For ultra-relativistic beams, i.e. $v \approx c$, the integrals for the wake potentials are independent of a parallel displacement of the path of integration. So the path may be shifted to the beam tube surface where the tangential electric and normal magnetic field components vanish. Then one needs to integrate only over the structure between the input and output of the beam tubes [10]. However, the version of MAFIA we are using does not provide the latter method. For the ion clearing electrodes simulations the direct method has been applied.

3.2.1 The geometry and meshing

The simulations are far more efficient if we make use of the inherent symmetry planes of the system. There are two planes of symmetry for the clearing electrodes structure, one in the x and one in the y direction. By selecting symmetry planes the size of the calculated region is reduced to one quarter and hence, the simulations will be smaller and solved more rapidly. For reproducibility and repeatability, the parameters of the geometry such as width and length of a gap are defined as

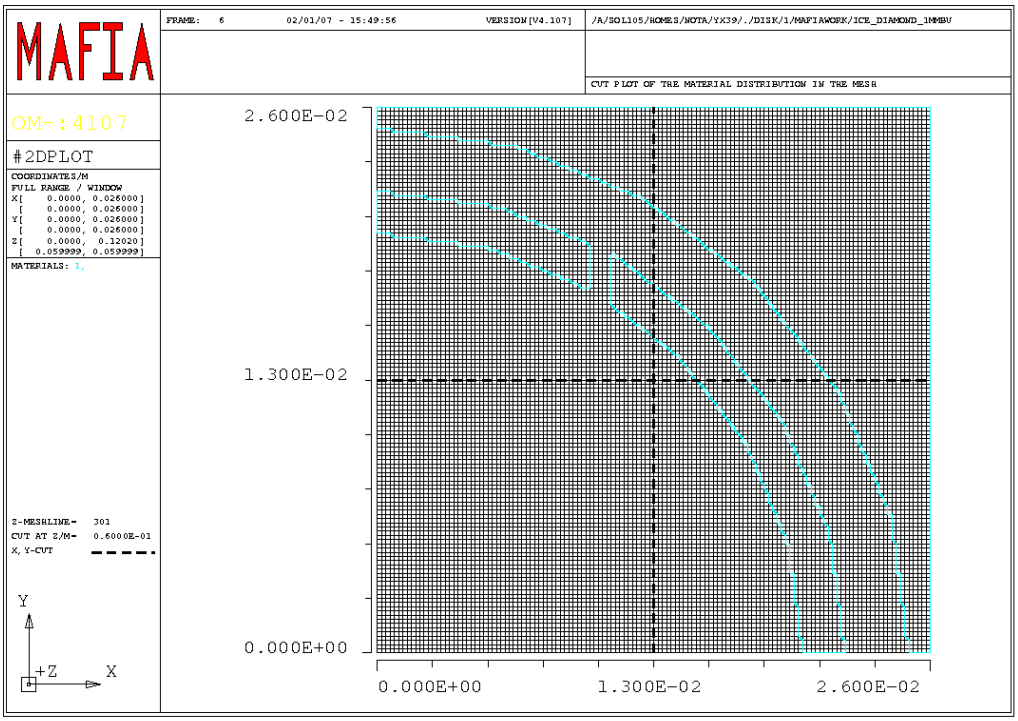

Figure 3.2: Meshing in MAFIA

variables. In this manner the models are quickly altered for the different structure dimensions, with the same simulation conditions initiated.

MAFIA does meshing in its M module. The mesh is the critical part, which controls the resolution and the accuracy of the results. In order to obtain an adequate resolution, at least 10 mesh cells per bunch length are required [11]. The ERL bunch length is 0.6mm in most of the accelerator, therefore it is required to have mesh cells at least 0.06mm in cell length. In the initial simulation, we were not able to do that due to memory limitations. The larger the mesh numbers the larger the amount of memory required, therefore the difficulties solving for larger structures with short bunch lengths is increasing incredibly.

MAFIA uses a quadrilateral mesh to model the geometry. Fig. 3.2 shows the meshes for a quarter cross-section of the ion clearing electrodes we designed.

3.2.2 Boundary conditions and particle beams

The main volume of the structure is vacuum and is bounded by perfectly conducting material, and the material for the ion clearing electrodes is also chosen to be perfectly conducting purely for simplicity. For this reason only the so-called geometric wake-field is calculated, which only depends on the structure geometry. The influence of resistivity in the walls is not considered. The entrance and exits to the beam pipes are perfectly matched ports in order to completely absorb the outgoing fields and to avoid any reflections at the port that would affect the wake-field calculations. In MAFIA, they are assumed to be open boundaries.

In MAFIA's time domain solver T3, the particle beams are treated as field sources such as finite line currents with charge density distribution longitudinally. For the longitudinal wake-field the beam travels through the center of the beam pipe. The beam has a Gaussian profile and is chosen to have a charge of one Coulomb for the calculation. The real charge is assigned during the post processing. The simulation runs long enough for the bunch to pass through the vacuum chamber structure with ion clearing electrodes and for its fields to decay.

3.2.3 Wake Monitors and post-processing

Monitors are set-up to store the longitudinal wake potential throughout the model. For the calculation of the loss factors, a test particle is chosen to be an arbitrary distance behind the particle and the resultant force on the particle determines its energy loss.

The monitors automatically store the longitudinal wake-potential. In order to calculate the corresponding loss factor an integration of this product of wake-potential and bunch profile is required. This is carried out during post-processing.

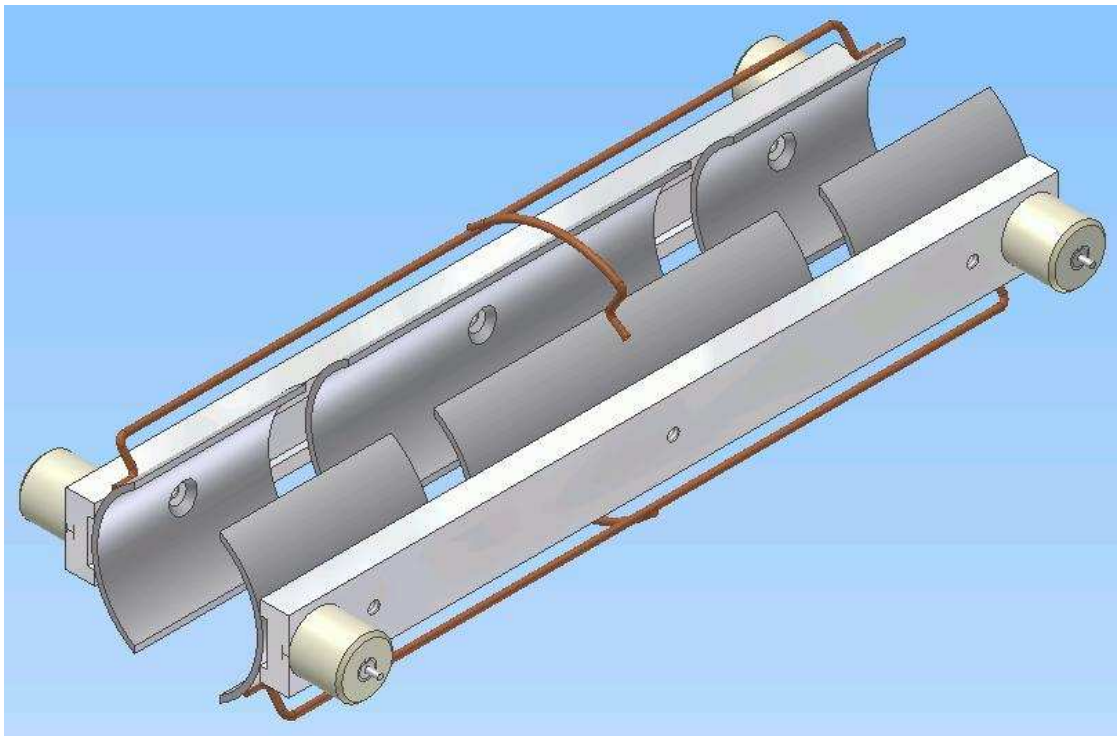

Figure 3.3: An ion clearing electrode from JLAB

3.3 Ion clearing electrodes from JLAB

I analyzed an ion clearing electrode design Fig. 3.3 from Thomas Jefferson National Accelerator Facility. The design was done for a much smaller beam current than ours.

Fig. 3.4 shows the 3D MAFIA model of that structure. Fig. 3.5 shows a comparison of using 5 meshes and 10 meshes per bunch length for a 5mm bunch length. Fig. 3.6 shows a comparison of using 5 meshes and 10 meshes per bunch length for a 1mm bunch length. We can observe some inaccuracies when the number of mesh points per bunch length gets smaller.

Fig. 3.7 shows the calculated wake potentials from 5mm bunch length to 1mm bunch length. Fig. 3.8 are the loss factors obtained by post-processing from Fig. 3.7. By fitting the loss factor data to a power law, we get the following relation

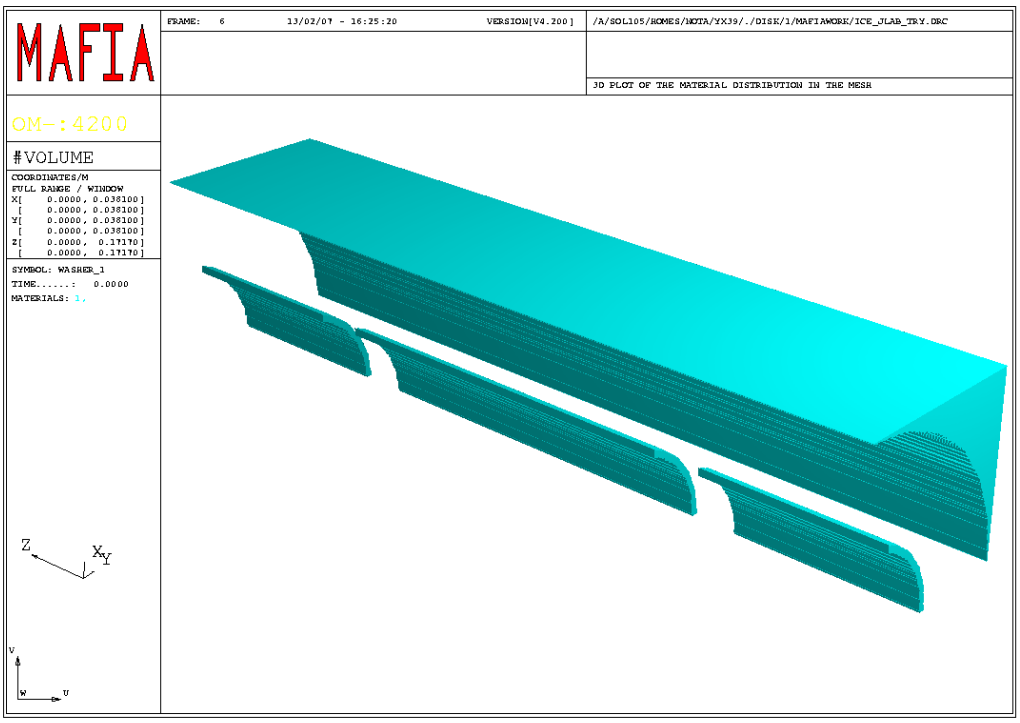

Figure 3.4: MAFIA model of an ion clearing electrode from JLAB

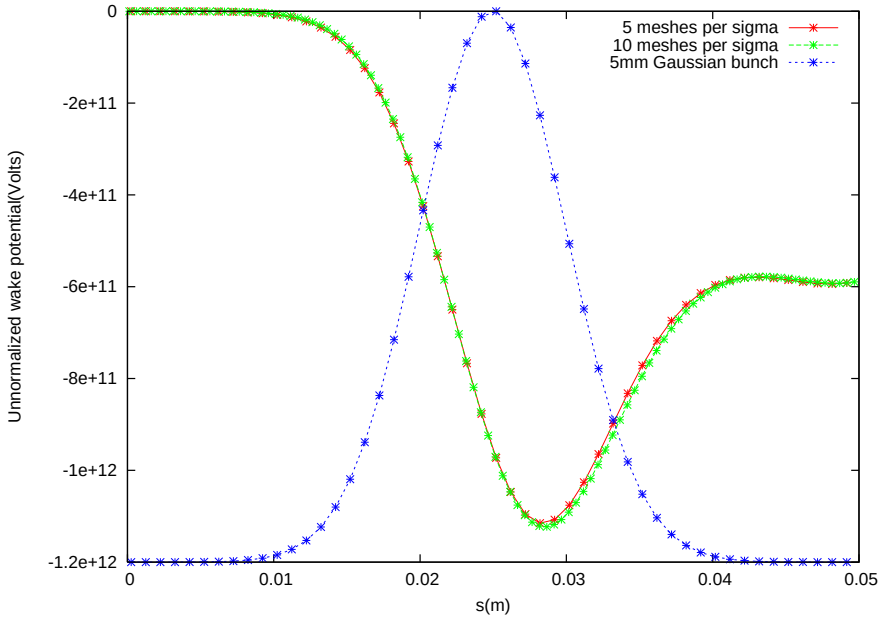

Figure 3.5: Mesh variation for a 5mm Gaussian bunch in Jlab ion clearing electrodes. Note that 5 mesh points per bunch length is sufficient in this structure.

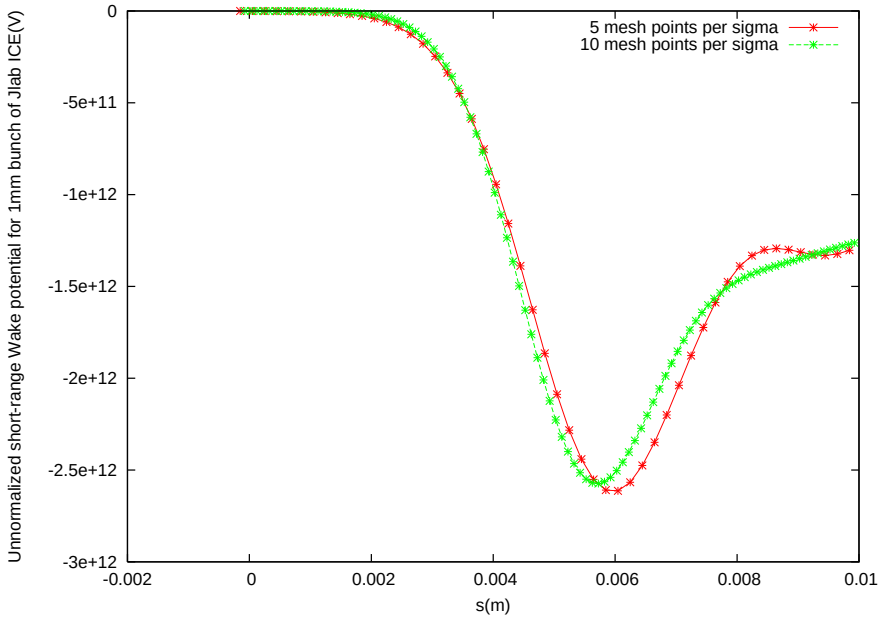

Figure 3.6: Mesh variation for a 1mm Gaussian bunch in Jlab ion clearing electrodes

between loss factor and Gaussian bunch length in that structure:

$$\kappa_{\parallel} = \frac{-1.80 \pm 0.02}{\sigma^{-0.49 \pm 0.01}}. \tag{3.13}$$

Here the unit of longitudinal loss factor is V/pC and the unit of Gaussian bunch length is mm. Therefore, for a 0.6mm bunch length, the loss factor is expected to be about -2.32V/pC. For the Cornell ERL project $I_{average} = 100$mA. The maximum bunch charge q_b is 77pC. So the heating power for such a structure is about $W = q_b \kappa_{\parallel} I_{average} \approx 17.9$W. Apparently that's not acceptable.

3.4 Initial design of ion clearing electrodes for the ERL

The shape of Fig. 3.9 has been designed by Yulin Li of LEPP for the ERL. The main difference between this design and JLAB's design is that it cuts the beam pipe wall with gaps and uses parts of the beam pipe as ion clearing electrodes.

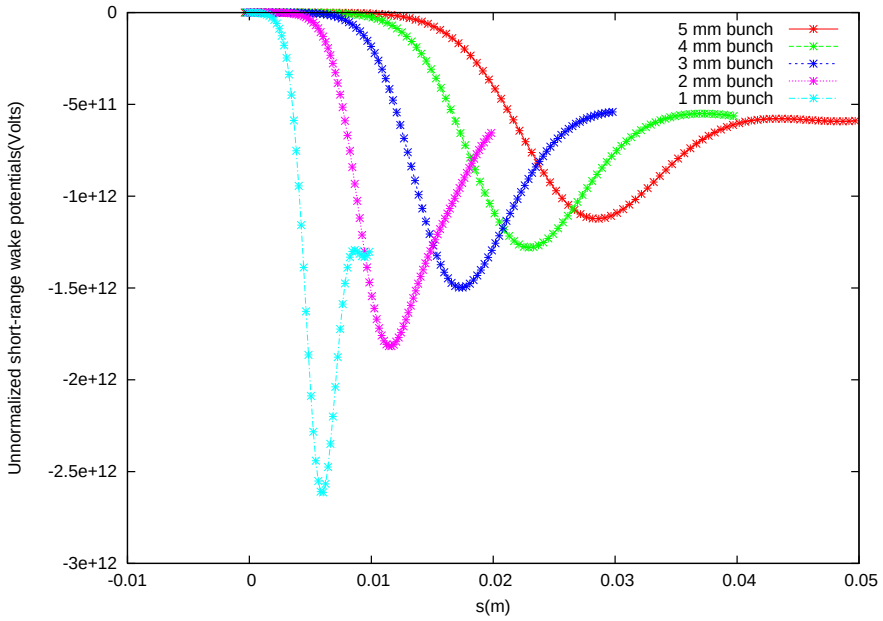

Figure 3.7: Wake potentials for different bunch lengths in Jlab ion clearing electrodes

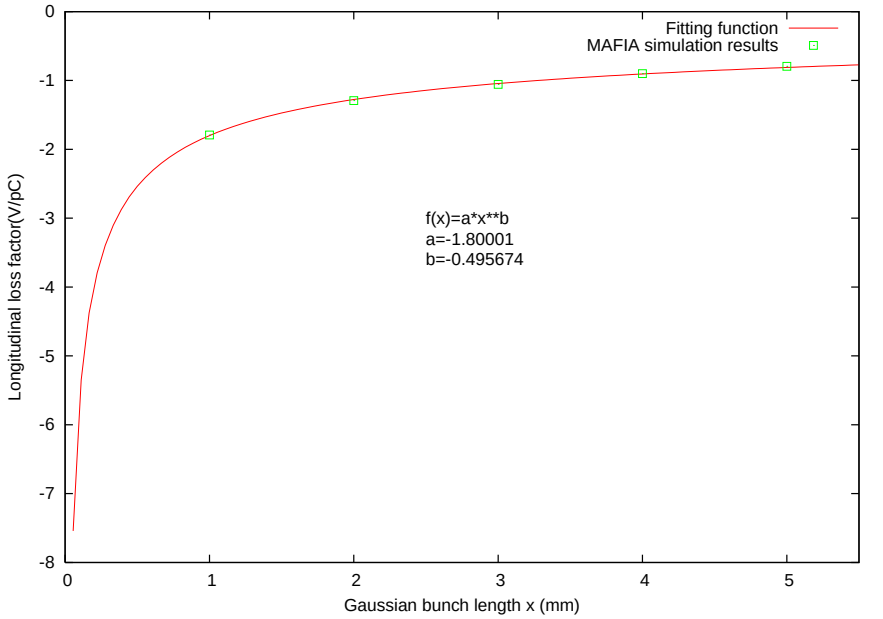

Figure 3.8: Longitudinal loss factors for different bunch lengths in Jlab ion clearing electrodes

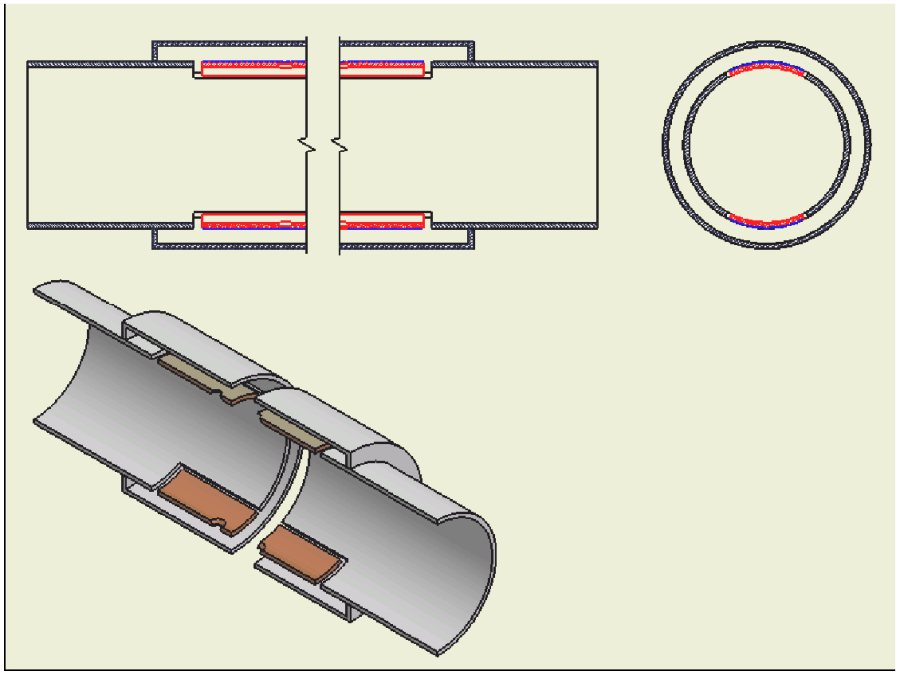

Figure 3.9: Ion clearing electrode for the ERL; design (1).

This may decrease the wake fields. Fig. 3.10 shows the MAFIA model of that structure.

Because this structure is longer compared to the previous JLAB's design, it's more time-consuming to conduct wakefield calculation using MAFIA. So we have used less than 10 mesh points per bunch length to get a rough estimate of how large wakefields would be. Fig. 3.11 shows the calculated wake potentials for 5mm bunch length to 1mm bunch length. Fig. 3.12 is the loss factors obtained by post-processing from Fig. 3.11. By fitting the loss factor data, we get the following relation between loss factor and Gaussian bunch length in that structure:

$$\kappa_{\parallel} = \frac{-2.97 \pm 0.05}{\sigma^{-1.45 \pm 0.05}}. \tag{3.14}$$

Here the unit of longitudinal loss factor is V/pC and the unit of Gaussian bunch length is mm. Therefore, for a 0.6mm bunch length of ERL, the loss factor

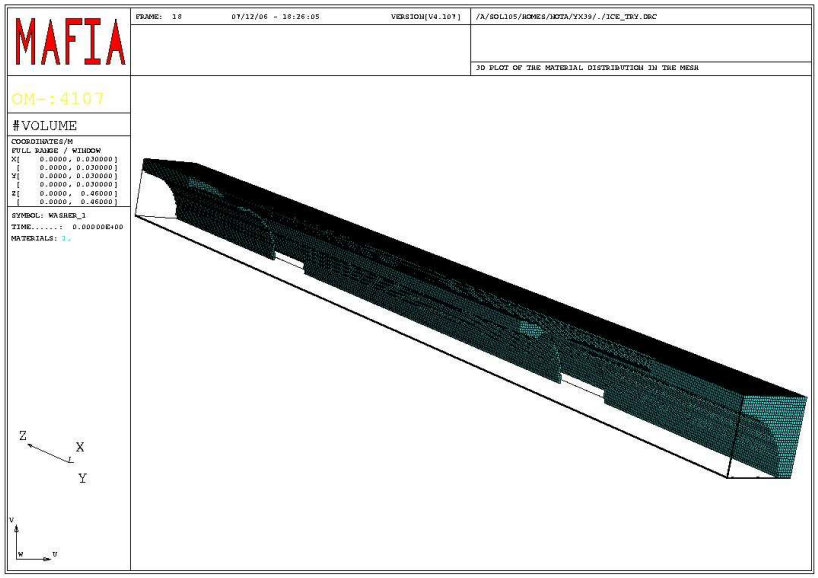

Figure 3.10: MAFIA model of the ion clearing electrode design (1)

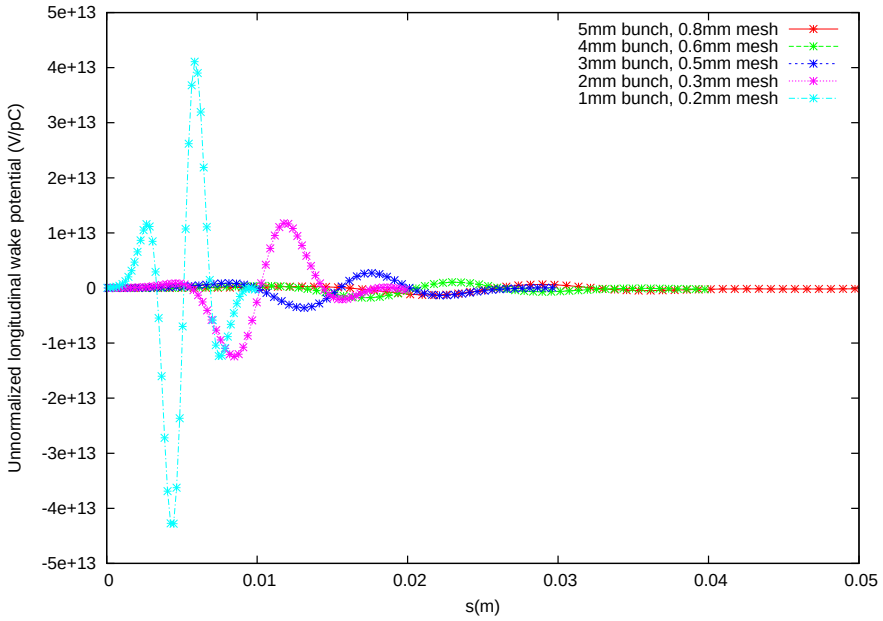

Figure 3.11: Wake potentials for different bunch lengths in ion clearing electrodes design (1)

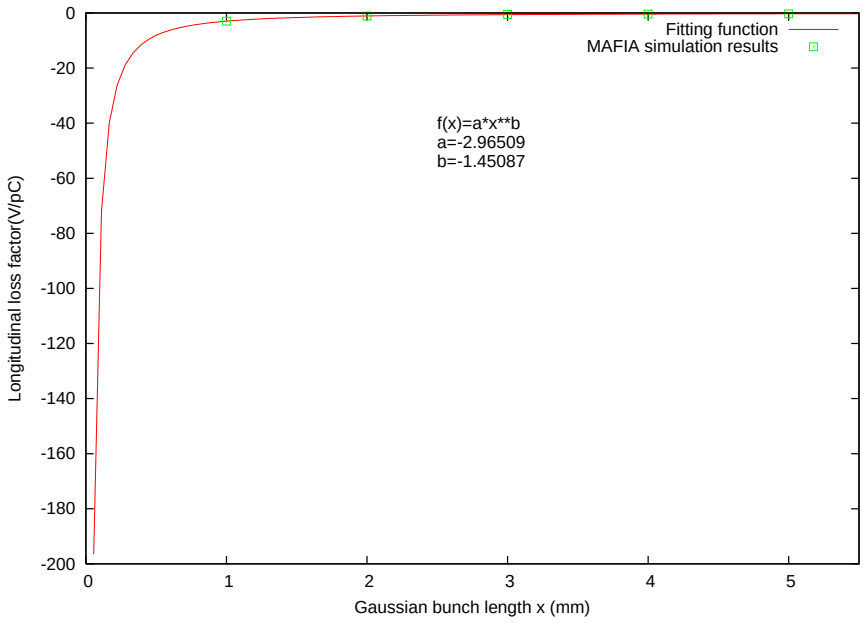

Figure 3.12: Longitudinal loss factors for different bunch lengths in ion clearing electrodes design (1)

is expected to be -6.22V/pC. For the Cornell ERL project $I_{average} = 100$mA. The maximum bunch charge q_b is 77pC. So the heating power for such a structure is about $W = q_b \kappa_{\|} I_{average} \approx 47.9$W. That's even worse than that for the Jlab design. The reason is that there're some transverse slots in the vacuum chamber wall that will greatly disturb the image current induced by the bunch.

In Fig. 3.11, there is a bump in the front part of the short-range longitudinal wakefield when 5 mesh points per bunch length was used for a 1mm Gaussian bunch. This bump is non-physical because the head of bunch must transfer energy to the tail of the bunch and therefore can not gain energy [12]. It can not gain energy from the structure because there is no power coupled to the structure from the outside. More about this non-physical bump will be discussed in Section 3.5.

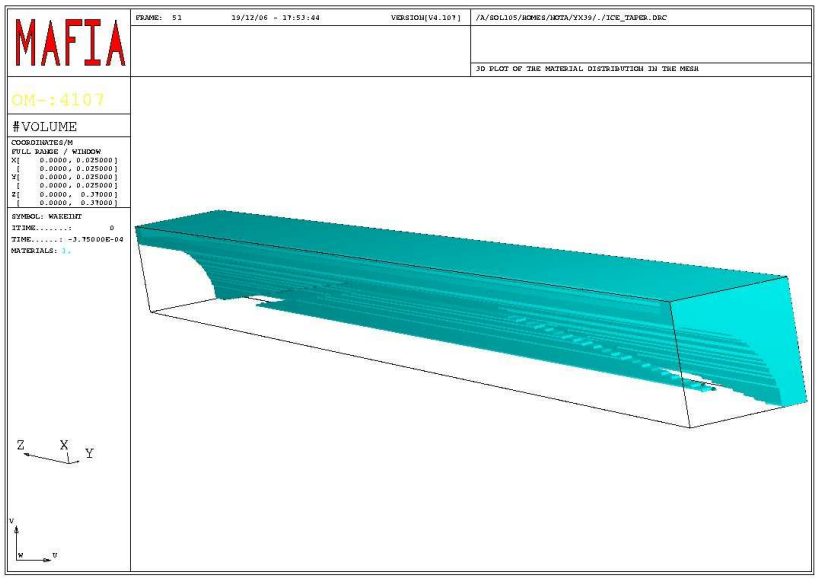

Figure 3.13: MAFIA model of a tapered clearing electrode design (2)

3.5 Tapered and diamond-shape ion clearing electrodes design

As we have mentioned before, transverse slots in the vacuum chamber is the main contribution to the wakefields of the design (1). So we tried to taper the clearing electrodes at both ends. Fig.3.13 shows such a design. Since the wakefields are mainly produced by the ends, our design evolves into a diamond-shape structure shown in Fig:3.14. Fig.3.15 is the 3-D view of one quarter of the diamond-shape structure generated by MAFIA.

Our simulation computer had been upgraded from 2 Gigabyte memory to 8 Gigabyte memory to enable us to do finer meshes simulations. We start from the standard procedure using 10 mesh points per bunch length. The following short-range longitudinal wake potential is shown in Fig. 3.16. Fig. 3.17 is the loss factors obtained by post-processing from Fig. 3.16. By fitting the loss factor data

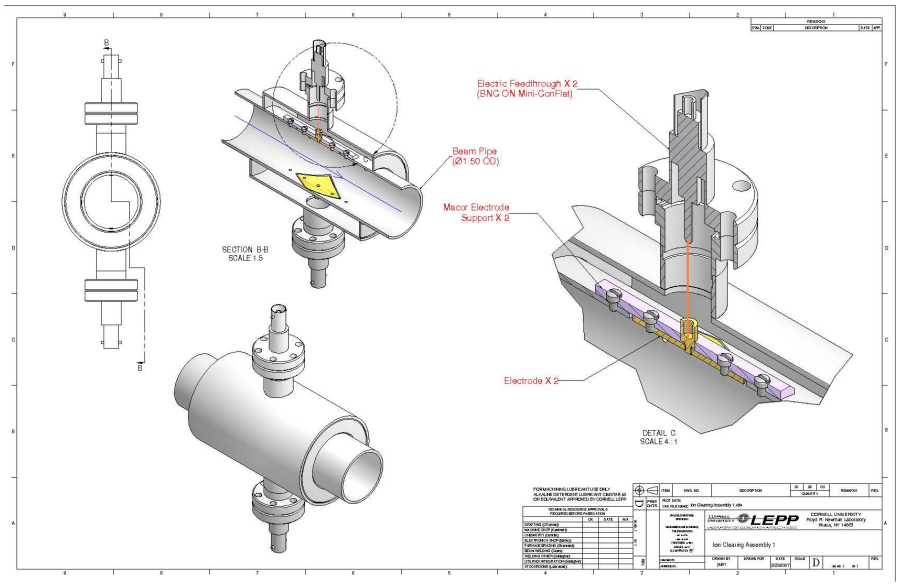

Figure 3.14: A diamond-shape clearing electrode design (2)

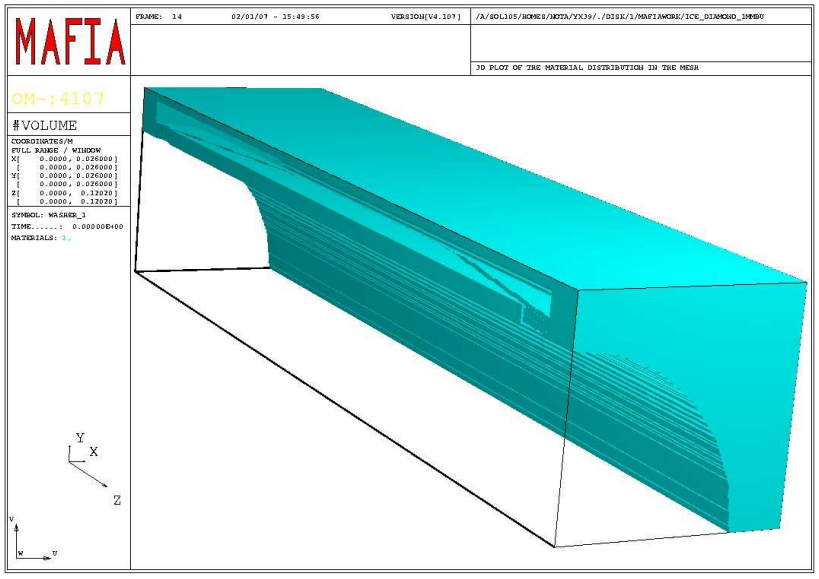

Figure 3.15: MAFIA model of the diamond-shape clearing electrode design (2)

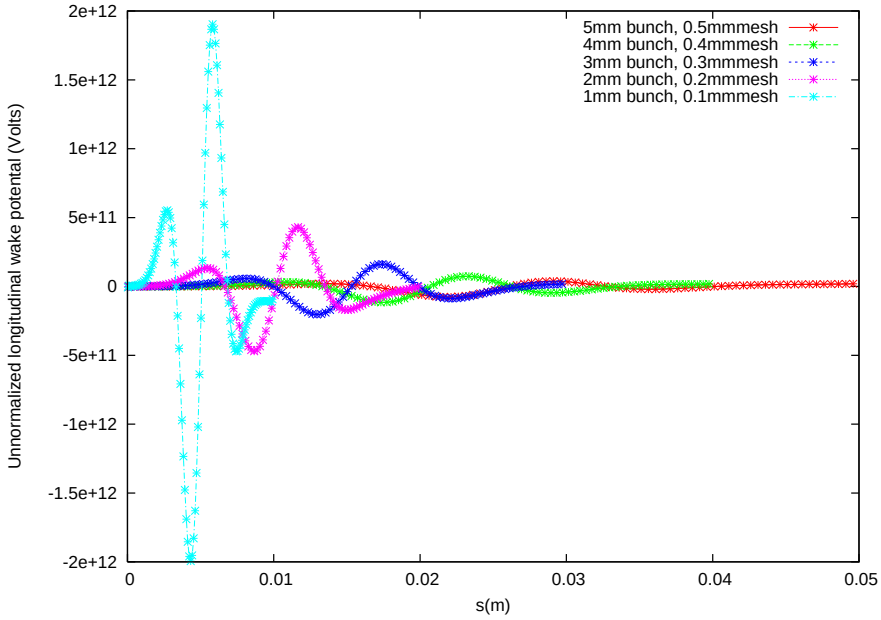

Figure 3.16: Longitudinal wake potentials for different bunch lengths in the diamond-shape clearing electrode, design (2)

to a power law, we get the relation Eqn. 3.15 between loss factor and Gaussian bunch length in that structure. Therefore for a 0.6mm bunch length of ERL, the loss factor is expected to be -0.14V/pC. So the heating power for such a structure is about 1.1W, far better than any of the two previous designs.

$$\kappa_{\parallel} = \frac{-0.08 \pm 0.01}{\sigma^{-1.10 \pm 0.13}} \tag{3.15}$$

3.5.1 Numerical dispersion errors

In Fig. 3.11, we have already observed some un-physical bumps in the front part of the longitudinal wake potential. This effect also appears when we use 10 mesh points per bunch length to calculate the diamond-shape clearing electrodes. With sufficient memory to construct a finer-mesh model, we used 20 or ever more mesh points per bunch length. Fig. 3.18 shows the longitudinal wake potentials for

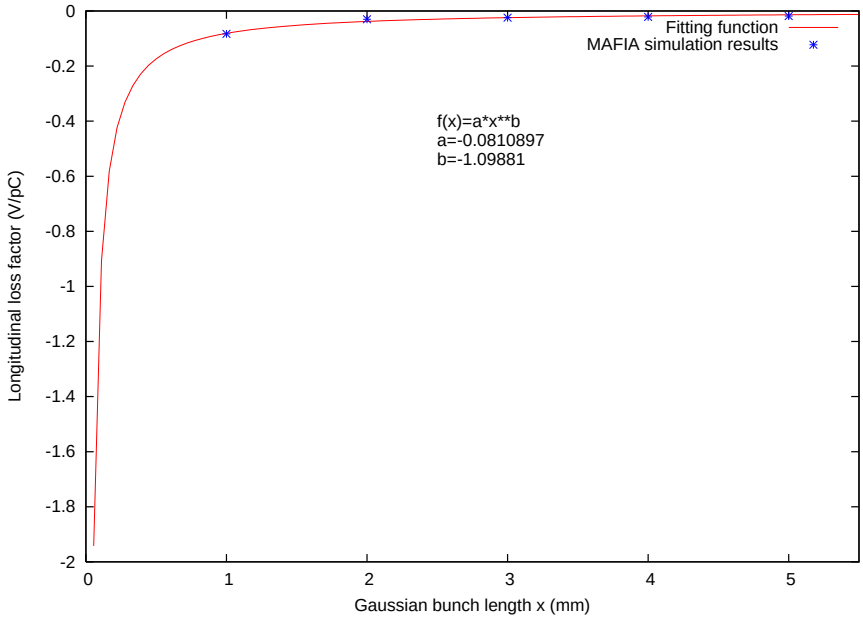

Figure 3.17: Longitudinal loss factors for different bunch lengths in the diamond-shape clearing electrode, design (2)

different mesh sizes. The un-physical bumps tend to decrease with the mesh size. The corresponding loss factors we obtained are shown in Fig. 3.19.

Other researchers have also reported this effect [13]. It is due to the dispersion error inherent in the Yee FDTD method MAFIA uses [14]. It is suggested [15] to use at least 35 mesh points per bunch length to overcome this effect. However, this requires much larger memories to get an accurate result.

3.5.2 Tapering effects

By decreasing the tapering angle while maintaining the gap width as 1mm, we can get more like longitudinal slots. Fig. 3.21 shows that the longitudinal loss factor per meter will get smaller if we decrease the tapering angle. When the tapering angle is getting smaller enough, the longitudinal loss factor per meter will not decrease too much because the diamond-shape clearing electrode is more like a

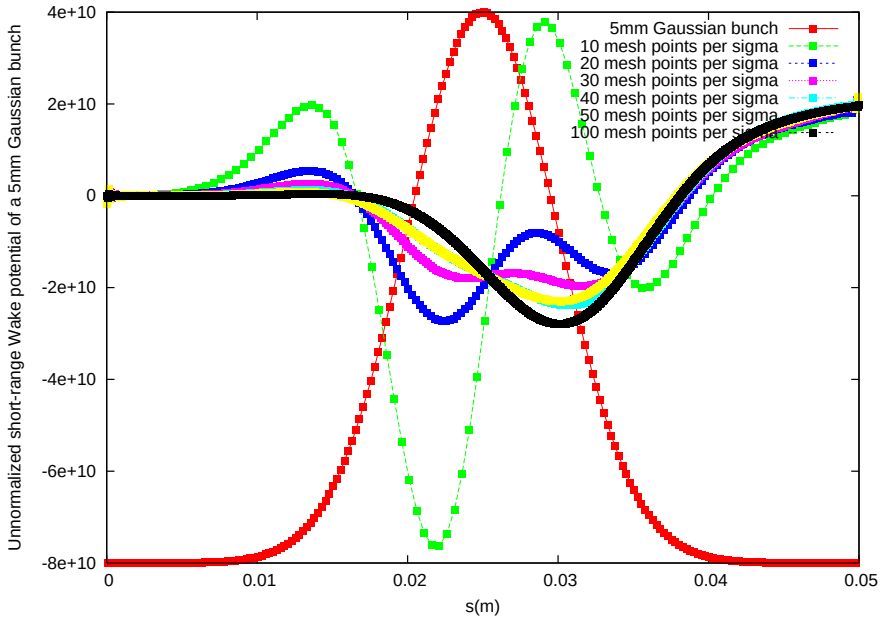

Figure 3.18: Longitudinal wakefields for different mesh sizes in MAFIA

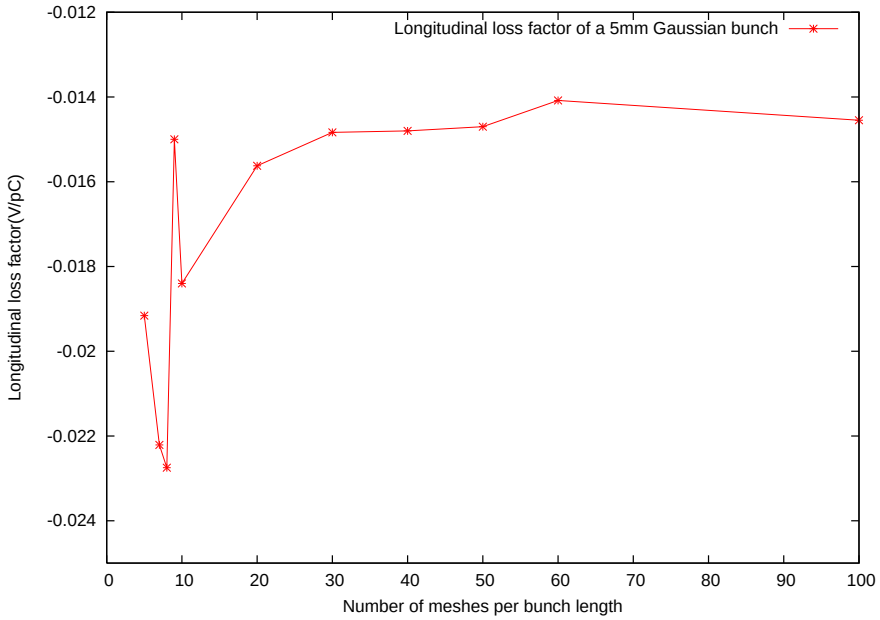

Figure 3.19: Longitudinal loss factors changed with the mesh size in MAFIA

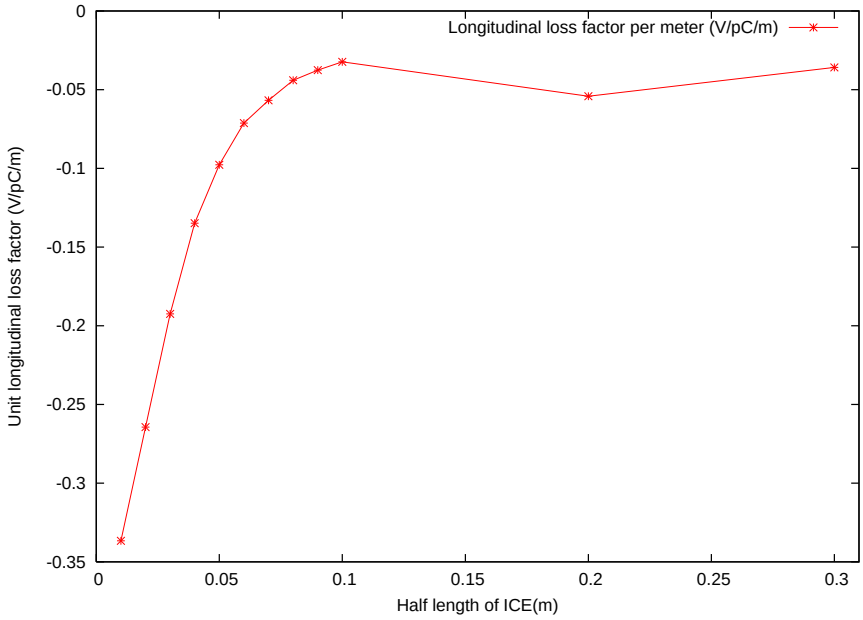

Figure 3.20: Longitudinal loss factor change with tapering angle in the diamond-shape clearing electrode

longitudinal slot now. According to [16], the longitudinal loss factor of a long slot does not depend on its length.

3.5.3 Gap width dependence

I now analyze the gap between the clearing electrodes and the beam pipe wall. Intuitively, if we increase the gap width, the electromagnetic field generated by the bunch will get reflected more. That means the wakefield effect will increase if we increase the gap width. Fig. 3.21 shows the relation between gap width and the longitudinal loss factor of a 5mm Gaussian bunch. It is therefore proposed to use a gap of 1mm.

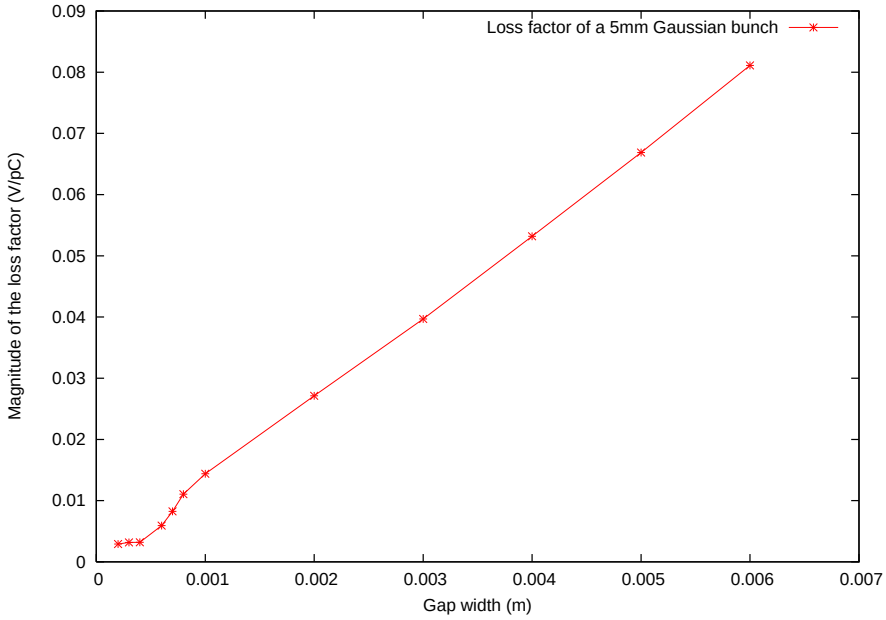

Figure 3.21: Longitudinal loss factor change with the gap width in the diamond-shape clearing electrode

3.6 A diamond-shape ion clearing electrode design with a smaller beam pipe radius

Since the beam vacuum pipe is not yet decided, I calculated a diamond-shape ion clearing electrode with a smaller beam pipe radius of 0.5 inch. The short-range wakefields can be seen as Fig. 3.22. The corresponding longitudinal loss factor is shown as Fig. 3.23. By fitting the loss factor data with a power law, we obtain the following relation Eqn. 3.16 between the Gaussian bunch length and the loss factor in that structure.

$$\kappa_{\parallel} = \frac{-0.08 \pm 0.01}{\sigma^{-0.84 \pm 0.04}} \tag{3.16}$$

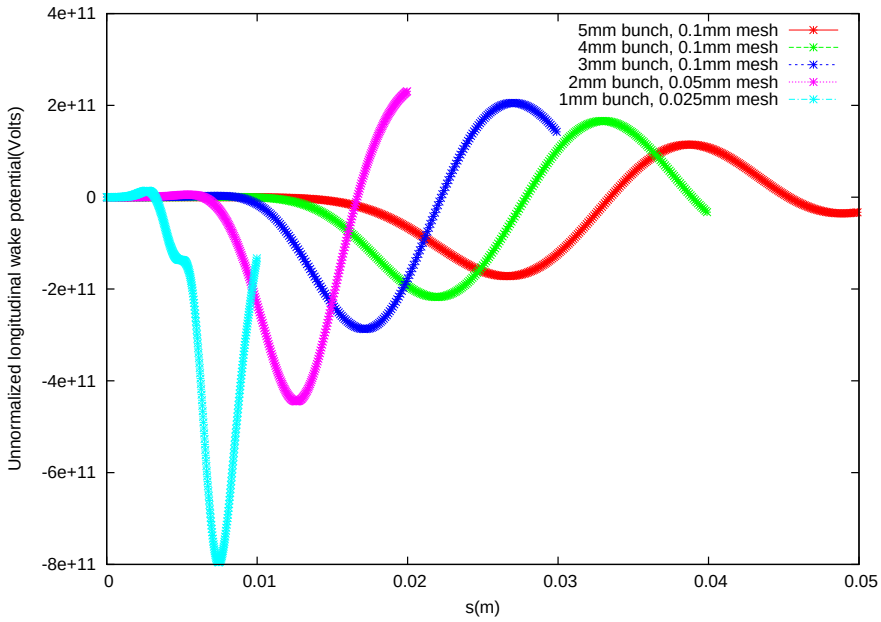

Figure 3.22: Longitudinal wake potentials for different bunch lengths in the diamond-shape clearing electrode with a smaller beam pipe radius, design (3)

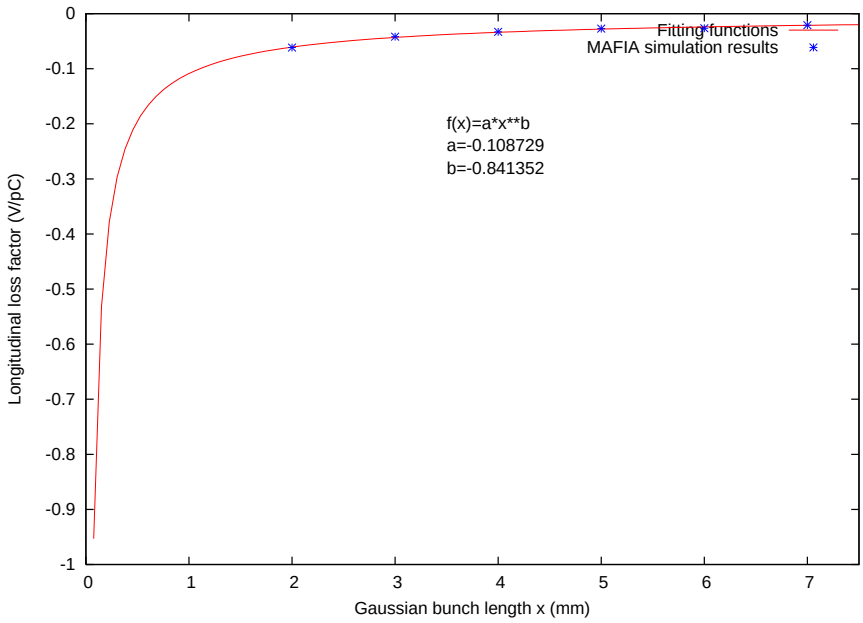

Figure 3.23: Longitudinal loss factors for different bunch lengths in the diamond-shape clearing electrode with a smaller beam pipe radius, design (3)

Chapter 4

Conclusion

We have calculated the electrostatic potential of an elliptical cross-section beam in a circular cross-section beam chamber along the Cornell ERL. By finding all the minimums of the beam potential, the locations of ion clearing electrodes are determined.

Different shapes of ion clearing electrodes are evaluated according to their short-range wakefields and loss factors. We have concluded that a diamond-shape ion clearing electrode can be used to minimize the heating power generated by the wakefields. The diamond-shape angle should be less than $acot10 \simeq 5.7°$, and the gap between the electrode and the wall should be approximately 1mm.

BIBLIOGRAPHY

[1] Donald H. Bilderback, Charles Sinclair and Sol M. Gruner, *"The Status of the Energy Recovery Linac Source of Coherent Hard X-rays at Cornell University"*; Vol.19, No.6, Synchrotron Radiation News(2006)

[2] A. Poncet, *"Ion trapping and clearing"*; unpublished note (1993)

[3] G. Hoffstaetter, M. Liepe, *"Ion Clearing in an ERL"*, Nuclear Instruments and Methods in Physics Research A 557, 205-212 (2006)

[4] Foster F.Rieke and William Prepejcha1, *"Ionization Cross sections of Gaseous Atoms and Molecules for High-Energy Electrons and Positrons"*, Phys. Rev. A 6, 1507 - 1519(1972)

[5] Y. Baconnier, G. Brianti, *"The stability of ions in bunched beam machines"*, Report CERN/SPS/80-2(DI) (1980)

[6] E. Regenstreif, *"Potential and field created by an elliptic beam inside an infinite cylindrical vacuum chamber of circular cross-section"*, Report CERN/PS/DL 77-37 (1977)

[7] B. Zotter, S. Kheifets, *"Impedances and wakes in high-energy particle accelerators"*, World Scientific, 1998

[8] N. Bakel et. al., *" A first study of wake fields in the LHCb vertex detector"*, LHCb note 99-041/VELO, (1999)

[9] MAFIA Collaboration, CST GmbH, Lautschlagerstr 38, 64289 Darmstadt

[10] S. Vaganian, H. Henke, *"The Panofsky-Wenzel theorem and general relations for the wake potential"*, Particle Accelerator 48, 239-242 (1993)

[11] C. Beard, R. Jones, *"Numerical simulations of collimator insertions using MAFIA"*, EUROTeV-Report-2006-103, (2006)

[12] M. Billing, private communications

[13] L. Bellantoni, G. Burt, *"Wakefield calculation for superconducting TM110 cavity without azimuthal symmetry"*, Fermilab-AB-TM-2356, (2006)

[14] A.Greewood et. al., *"On the elimination of numerical cerenkov radiation in PIC simulations"*, Journal of Computational Physics 201 (2004) 665-684

[15] G. Burt, private communications

[16] G. Stupakov, *"Coupling impedance of a long slot and an array of slots in a circular vacuum chamber"*, Physical Review E, 51, 3515 - 3521(1995)